Chapter 3

Laser guiding

"Computers are useless. They can only give you answers." Pablo Picasso

This chapter will describe how a laser beam can be used to efficiently guide a cold atomic cloud. Work contained within this chapter led to the publication of ref. [141] and has been carried out in collaboration with the other authors.

3.1 Gaussian laser beam profile

For laser light, with power P, traveling along the z-axis, with a radially symmetric Gaussian transverse profile, the form of the intensity is:

$$I(r,z) = \frac{2P}{\pi w(z)^2} \exp\left(\frac{-2r^2}{w(z)^2}\right), \tag{3.1}$$

where $r = \sqrt{x^2+y^2}$. The $1/e^2$ intensity radius of the beam, $w(z)$, is the radial distance from the z-axis to the point where the intensity has decreased by a factor of e^2 ($= 7.389$), and is given by:

$$w(z) = w_0 \sqrt{1 + \left(\frac{z-z_0}{z_\mathrm{R}}\right)^2}. \tag{3.2}$$

Here w_0 is the beam waist[1], z_0 is the focal point, and z_R is the Rayleigh length, given by:

$$z_\mathrm{R} = \frac{\pi w_0^2}{\lambda_\mathrm{T}}. \tag{3.3}$$

The Rayleigh length is a measure of the length scale of the diffraction that is introduced via eqn. (3.2). It is the axial distance required for the laser beam's area to double in size. The quantities parameterising a Gaussian beam are shown in Figure 3.1.

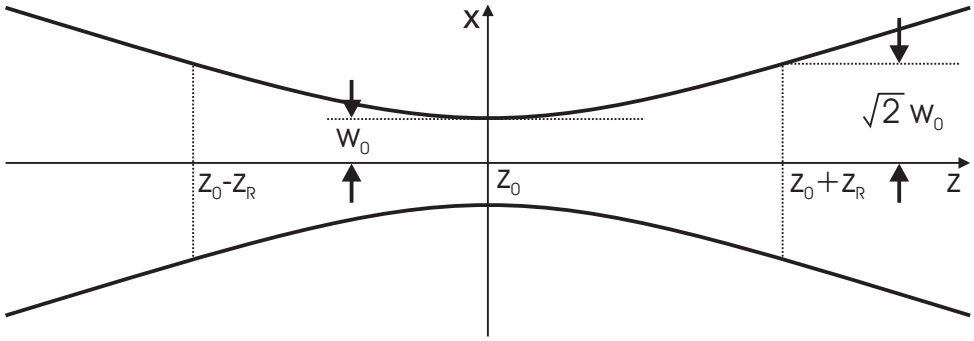

Figure 3.1: Diagram showing the important quantities that define a Gaussian laser beam. The thick black lines indicate the $1/e^2$ radius. The diagram is a cut through the $y = 0$ plane.

3.2 Laser guide modelling

In this chapter a specific experimental setup is modelled, however the analysis can be easily applied to other setups. Figure 3.2 (a) shows a diagram of the guiding experiment. A Magneto-optical trap (MOT), centred at $\{0, 0, 0\}$, collects cold ^{85}Rb atoms at a temperature of $\mathcal{T} = 20.0$ μK (with corresponding velocity standard deviation $\sigma_V = \sqrt{k_\mathrm{B}\mathcal{T}/m} = 4.42$ cm s^{-1}) and with an isotropic Gaussian spatial distribution in each Cartesian direction, with standard deviation of $\sigma_R = 0.20$ mm. The atoms are launched vertically upwards as a fountain using the moving molasses technique [142]. The initial launch velocity is chosen so that the centre of mass parabolic trajectory will have an apex at a height of $h = 22.0$ cm above the MOT centre. This requires a

[1]The use of the term 'beam waist' to measure a radius is misleading. However, as the term is in common use, this terminology will be adopted.

launch velocity of $v_{z_i} = \sqrt{2gh} = 2.08$ m s^{-1}. The MOT to apex flight time is $T = \sqrt{2h/g} = 212$ ms. At 18.0 cm above the MOT there is a 0.5 mm radius aperture, to allow the atoms to pass into a lower pressure 'science' chamber (typically 2 orders of magnitude lower pressure). The time to reach the aperture is 121 ms for unperturbed motion.

A vertically oriented red-detuned laser provides radial guiding via the optical dipole force. The dipole trap depth is proportional to the laser power. Therefore a far-detuned guiding experiment (with negligible scattering) will always have more efficient loading by increasing the laser power. A Nd:YAG ($\lambda_T = 1,064$ nm) guide laser that has a maximum power of 19 W was chosen to be modelled. These parameters match a similar experiment conducted by Davies *et al.* [75]. The beam waist and focal point are chosen to optimise the guiding efficiency, and this optimisation process is contained in Section 3.3.

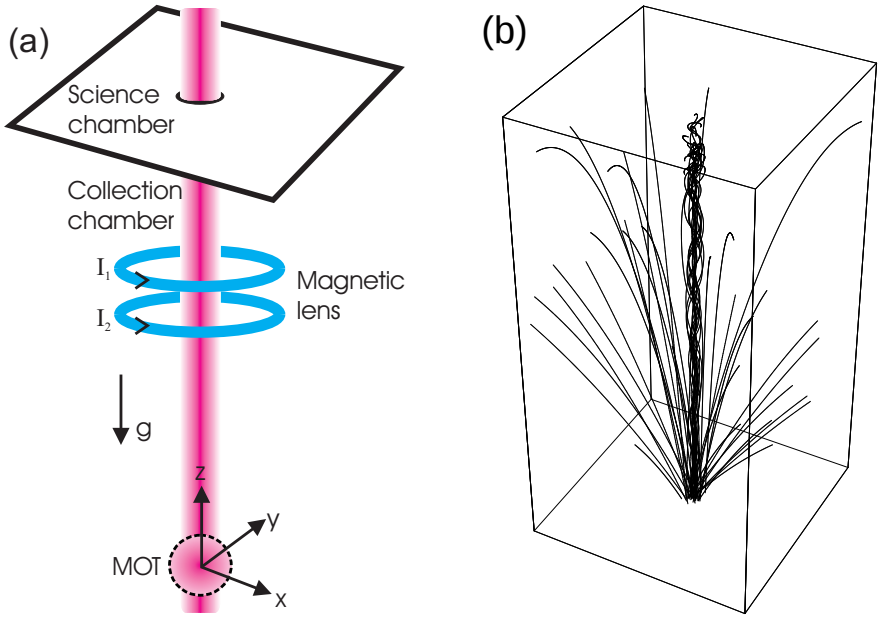

Figure 3.2: Diagram (a) shows the experimental setup with guiding laser beam, magnetic lens and aperture for differential pumping. Atoms are collected in a MOT and then launched vertically. In (b) a numerical simulation shows the trajectories of launched atoms. Roughly 30% of the atoms are guided within the laser beam, these constitute the central column of the simulation. The unguided atoms follow ballistic trajectories.

In Figure 3.3 (a) and (b) the Rayleigh length and the $1/e^2$ radius at the aperture height of 18.0 cm are plotted against beam waist for the simulated experiment. The minimum $1/e^2$ radius at the aperture occurs when the Rayleigh length

equals the aperture height. From eqn. (3.2) the minimum beam radius is $w(z) = \sqrt{2}w_0$.

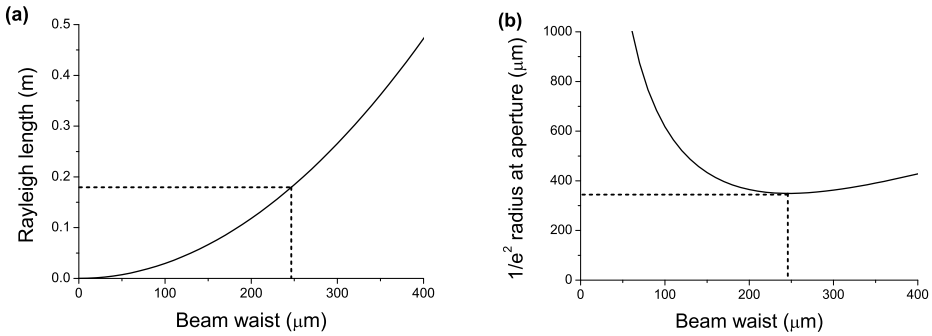

Figure 3.3: Plot (a) shows the Rayleigh length (eqn. (3.3)) plotted against beam waist w_0. In (b) the $1/e^2$ radius at the aperture height ($z = 18.0$ cm) is plotted against beam waist. The minimum of 349 μm occurs when $z_{\mathrm{R}} = 18.0$ cm.

3.2.1 The dipole force

Combining the expressions for the dipole potential (eqn. (2.1)) and the laser intensity (eqn. (3.1)), gives the potential an atom in the ground state experiences:

$$U_{\mathrm{Dip}}(r,z) = -\frac{\alpha_0 P}{\epsilon_0 c\,\pi\, w(z)^2} \exp\left(\frac{-2r^2}{w(z)^2}\right), \tag{3.4}$$

Using $\alpha_0 = (4\pi\epsilon_0) \times 693.5\ a_0^3$ C m^2 V^{-1} for Rb in the presence of $\lambda_{\mathrm{T}} = 1.064$ μm light [140], a 19 W laser with a beam waist of 250 μm (peak intensity of 1.94×10^8 W m^{-2}) produces a trap depth of $U_{\mathrm{Dip}}/k_{\mathrm{B}} = 30.2$ μK. The force an atom experiences due to the laser guide is given by $\mathbf{F}_{\mathrm{Dip}} = -\nabla U_{\mathrm{Dip}}$. The radial and axial accelerations for a ^{85}Rb atom have been plotted in Figure 3.4. The radial acceleration is comparable with g and 3 orders of magnitude larger than the axial case. It is sufficiently large to provide an adequate guide for the cold atoms. On the contrary one wouldn't expect to see much evidence of perturbation from the ballistic motion in the axial direction. The length scales over which the radial and axial accelerations change are characterised by the beam waist and the Rayleigh length respectively. The radial angular frequency

for the laser guide is given by:

$$\omega_{r_{\rm L}} = \sqrt{\frac{4\alpha_0 P}{m\,\epsilon_0 c\,\pi\,w(z)^4}}\ . \tag{3.5}$$

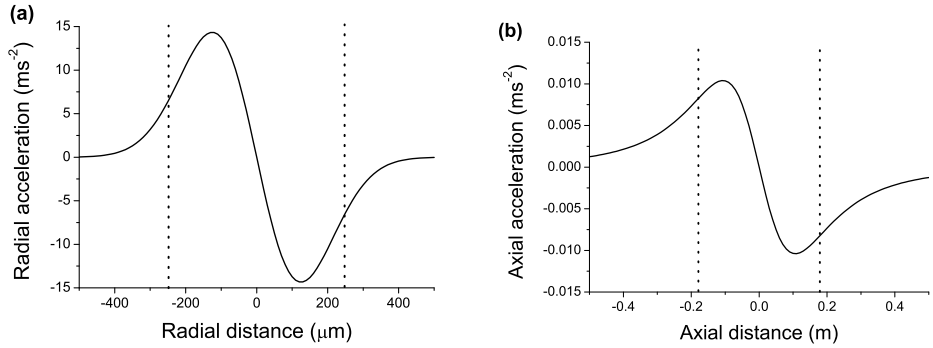

Figure 3.4: In plots (a) and (b) the radial and axial accelerations are plotted against distance from the beam centre. A 19 W laser with beam waist of 250 μm is used in the calculation. The radial acceleration is $\sim 10^3$ times larger than the axial case. The dashed vertical lines in (a) and (b) are $\pm w_0$ and $\pm z_{\rm R}$ respectively.

3.2.2 Computer simulation

The expression for the force can be used in a numerical simulation of atomic trajectories within the laser guide. The computer program generates an atomic cloud made up of atoms that have random positions and velocities, the Gaussian distribution of which match the standard deviations given earlier. It is assumed that the only perturbations that the atoms experience are a downwards force due to gravity and the dipole potential. The effect of heating due to light scattering is negligible. A calculation for the above parameters, using eqn. (2.4), gives a scattering rate of ~ 0.1 photons per second. Collisions can be ignored as the average elastic collision rate within the MOT is 3 s^{-1}, see the calculation in Appendix E. The atoms are treated as point like particles, moving classically due to a force that is derived from quantum mechanics. The numerical solving of the differential equations was performed by *Mathematica*. A sample program to aid the understanding of the program has been included in Appendix F.

3.3 Loading the guide

Calculating the guiding efficiency can be broken down into two separate problems: loading atoms from the MOT into the guide, and subsequent transport losses. The fraction of atoms initially captured by the laser beam can be calculated analytically based on the work of Pruvost *et al.* [77] and extended by Wolschrijn *et al.* [143]. An atom will be radially bound if its total energy E is less than zero:

$$E = \frac{p^2}{2m} + U_{\mathrm{Dip}}(r, z) < 0, \tag{3.6}$$

where $p = \sqrt{{p_x}^2 + {p_y}^2}$ is the radial momentum and m is the atomic mass.

The initial atom distribution can be divided into two groups: energetically bound ($E < 0$) and unbound ($E > 0$). The normalised initial position and momentum distribution of the atomic cloud for a given temperature $\mathcal{T}$ is given by:

$$\Phi(r, p) = \frac{e^{-r^2/2{\sigma_R}^2}}{2\pi{\sigma_R}^2} \frac{e^{-p^2/2mk_B\mathcal{T}}}{2\pi m k_{\mathrm{B}}\mathcal{T}}. \tag{3.7}$$

The momentum standard deviation is given by: $\sigma_P = m\,\sigma_V = \sqrt{mk_{\mathrm{B}}\mathcal{T}}$. The loading efficiency, χ, is calculated by integrating $\Phi(r, p)$ and imposing the bound condition of eqn. (3.6) as the momentum integration limit:

$$\chi = \int_0^\infty \int_0^{\sqrt{2mU_{\mathrm{Dip}}(r,z)}} \Phi(r, p)\; 2\pi r\; \mathrm{d}r\; 2\pi p\; \mathrm{d}p. \tag{3.8}$$

By using the substitution $q = e^{-2r^2/w(z)^2}$ for the second integral, the solution is:

$$\chi = 1 - \frac{w(z)^2}{4{\sigma_R}^2} \left(\frac{\alpha_0 P}{\epsilon_0 c\,\pi\, w(z)^2 k_{\mathrm{B}}\mathcal{T}} \right)^{-\frac{w(z)^2}{4{\sigma_R}^2}} \Gamma\left(\frac{w(z)^2}{4{\sigma_R}^2}, 0, \frac{\alpha_0 P}{\epsilon_0 c\,\pi\, w(z)^2 k_{\mathrm{B}}\mathcal{T}} \right), \tag{3.9}$$

where $\Gamma(a, b, c) = \int_b^c q^{a-1} e^{-q}\, \mathrm{d}q$ is the generalised incomplete gamma function. The loading efficiency is plotted against beam waist and focal point in Figure 3.5 (a). The optimum $1/e^2$ radius for loading the modelled experiment is 252 μm, and this produces a load efficiency of 28.9%. The maximum exhibits a large plateau ($\chi > 25\%$ when the $1/e^2$ radius is between 175 μm and 360 μm) which results in great flexibility in choosing initial parameters. Due to this flexibility it was decided to study laser guiding when the beam focus coincides

with the MOT centre ($z_0 = 0$ cm). The reason for this is that an expanding beam will cool the cloud in the radial direction during the flight [77]; this is a consequence of Liouville's theorem [144]. For the rest of this thesis, all results presented will use a laser that is focused on the MOT centre, see Figure 3.5 (b). Alongside the analytical result, a Monte Carlo simulation of atomic trajectories was performed by solving the equations of motion that include gravity and the dipole force. The data points on the plot show the fraction of atoms from the MOT that are initially energetically bound and therefore satisfy eqn. (3.6).

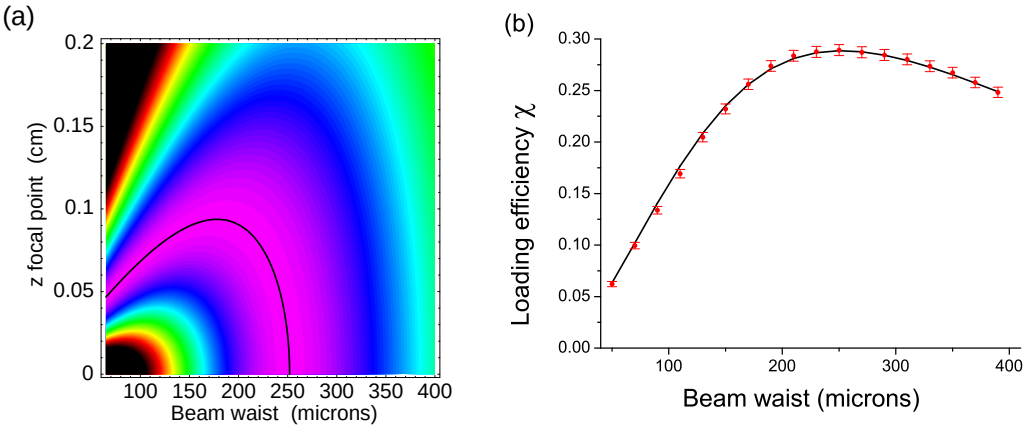

Figure 3.5: Plot (a): The analytical load efficiency, χ, is plotted against beam waist and z focal point. The black contour represents the optimum $1/e^2$ beam radius of 252 μm which corresponds to a load efficiency of 28.9%. Plot (b): The $z_0 = 0$ cross section of (a). The solid line is the analytical result and the data points are the result of a numerical simulation consisting of 10,000 atoms.

The loading efficiency can be increased by using a more powerful laser, a lower temperature atomic cloud or a smaller cloud size. The first two are intuitively obvious, however the reduction in cloud size is misleading because atom number is the important experimental quantity one wishes to maximise. For a MOT with constant atom density, the atom number increases proportional to the cube of the cloud radius. Although for large clouds a smaller cloud fraction is loaded, there is a greater number of atoms present and therefore the overall load increases with cloud radius.

3.4 Transport losses

Having considered the initial loading of the MOT into the laser beam, attention is now turned to the guiding properties and losses from the beam. Apart from heating and collisions (which are assumed to be negligible) there are two loss mechanisms: aperture truncation and diffraction.

3.4.1 Truncation losses

Without laser guiding, the transmission from a ballistically expanded cloud passing through a 0.5 mm radius aperture at a height of 18 cm is 0.4%. With guiding, this transmission can be increased by 75 times. This is shown in Figure 3.6 (a) where the transmission through the aperture is plotted against height above the MOT. The black line represents the transmission of an unguided atomic cloud. The aperture height of 18.0 cm was chosen to minimise ballistic transmission but still allow sufficient distance between the aperture and trajectory apex at 22 cm. The red and blue lines demonstrate laser guiding for 100 μm and 250 μm beam waists respectively. Again there is the initial decay due to the unguided atoms passing through the aperture. However, unlike the unguided case, a fraction of the atoms have been bound in the laser guide which significantly increases the aperture transmission. This corresponds to the tight core evident in Figure 3.2 (b). There is also atom loss from the guide due to diffraction. This is more obvious in the tightly focused 100 μm beam (red line), although all expanding laser beams will suffer losses. This diffraction loss is examined in Section 3.4.2.

In Figure 3.6 (b) there is a plot of transmission versus aperture radius at 18.0 cm above the MOT centre. The sharp spike in the distribution is the guided atoms and the broader distribution is due to the ballistically expanded atomic cloud. The aperture size should be large enough to allow the guided atoms to pass through unhindered. The highest achievable loading efficiency for the setup modelled has a beam radius of $w(z) = 349$ μm at the aperture. The $1/e^2$ radius is twice the radial standard deviation: $w(z) = 2\sigma_r$. With this definition the beam radius is $\sigma_r = 175$ μm and therefore the 0.5 mm aperture has a radius of 2.86 σ_r, corresponding to a 99.6% transmission through the aperture. A much

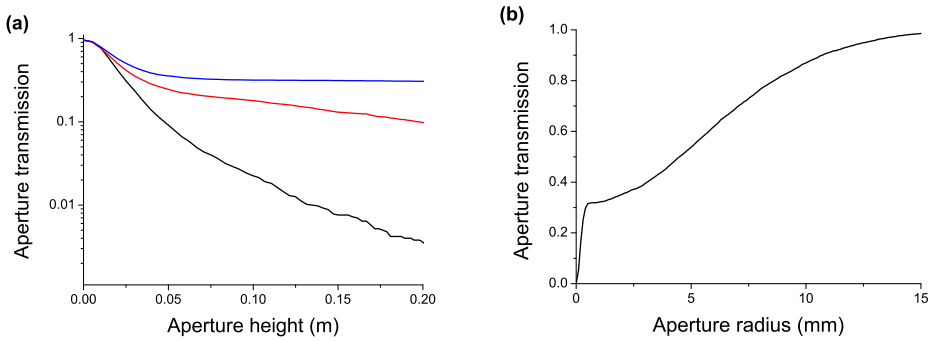

Figure 3.6: Plot (a): Transmission through a 0.5 mm radius aperture is plotted against aperture height above the MOT centre. The black line is with no laser present, the red line is with a laser of waist 100 μm and the blue line is with a 250 μm waist. Plot (b): The transmission is plotted against aperture radius for an aperture at a height of 18.0 cm above the MOT. The distribution consists of a tightly guided core due to a laser of waist 250 μm and the ballistically expanded cloud (σ_r = 5.4 mm). The simulation follows the trajectories of 5,000 atoms to obtain the aperture transmission.

larger beam radius could result in high losses when passing through the small aperture.

3.4.2 Diffraction losses

Away from the focus, diffraction causes the guiding potential to relax. For some bound atoms this can mean their kinetic energy becomes larger than the depth of the confining potential - the atoms are therefore lost from the guide. Ideally a transportation scheme requires a laser profile that doesn't change size on the scale of the guiding distance. The Rayleigh length is a good measure of this, and therefore for efficient guiding one must ensure that the transport distance is on the order or less than the Rayleigh length. A Monte Carlo simulation of 5,000 atoms being transported within the laser guide was run to investigate the loss due to diffraction. In Figure 3.7 (a) the red data points are the ratio of the number of energetically bound atoms at the aperture to the number of initially bound atoms. For small beam waists the Rayleigh length is much smaller than the transport length and the increased diffraction reduces the transport efficiency.

The overall transport efficiency is shown in Figure 3.7 (b). In this plot the fraction of atoms passing through the aperture is plotted against beam waist. In

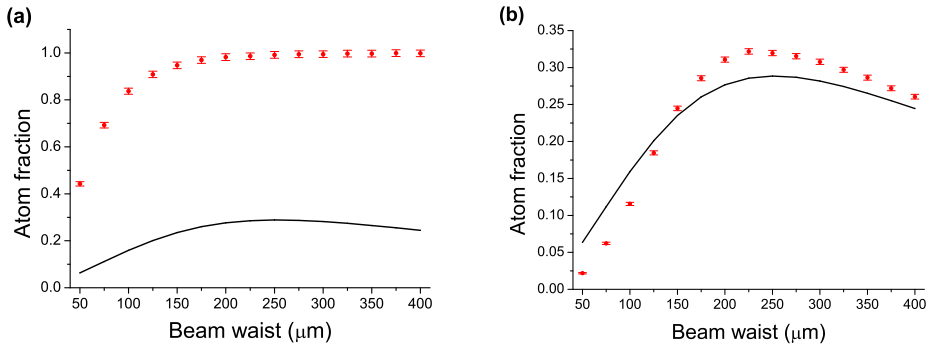

Figure 3.7: Plot (a): The ratio of the number of energetically bound atoms at the aperture to the number of initially bound atoms is plotted against beam waist. Values less than one represent losses due to diffraction. Plot (b): The fraction of atoms passing through the aperture (transport efficiency) is plotted against beam waist. The quantity represents the overall transport efficiency. The solid line in both plots is the loading efficiency χ given by eqn. (3.9).

addition to the fraction of bound atoms passing through the aperture (obtained by multiplying the two curves in Figure 3.7 (a)), there is an extra contribution from nearly bound atoms that have been 'funneled' through the aperture. Those nearly bound were either just outside the bound criteria of eqn. (3.6) at the initial MOT loading, or have been lost from the guide due to diffraction. Their trajectories loosely follow the laser guide, and therefore there is an increased probability of passing through the aperture. Simulations show that the distribution of unbound atoms that are transmitted through the aperture peaks at 6%, which accounts for the extra 4% contribution to the transport efficiency curve in Figure 3.7 (b). The peak in the unbound atom distribution is centred at a smaller beam waist, due to the unbound atoms having a hotter temperature than their bound counterparts. This explains why the transport efficiency curve has its peak shifted to 225 μm.

It is instructive to look at phase-space plots to get an understanding of the initial capture and subsequent loss due to diffraction, see Figure 3.8. The left (right) column simulates a laser with a 100 μm (250 μm) beam waist. The diffraction of the laser beam can be seen by studying the evolution of the thick red $E = 0$ contour. The 250 μm beam provides a better guide as it both captures more atoms initially and suffers from less diffraction loss. In both plots the nearly bound atoms can be seen just outside the $E = 0$ line. It takes a finite time for them to be ejected from the guide. It is these atoms that are the extra contribution in Figure 3.7 (b).

Chapter 3 summary

- The Gaussian laser intensity profile was described.
- A numerical simulation of an experiment to guide a vertically launched atomic cloud was outlined.
- An analytical formula for guide loading was derived. The beam parameters were optimised to produce a loading efficiency of 28.9% into the guide.
- The truncation and diffraction loss mechanisms from the guide were investigated.

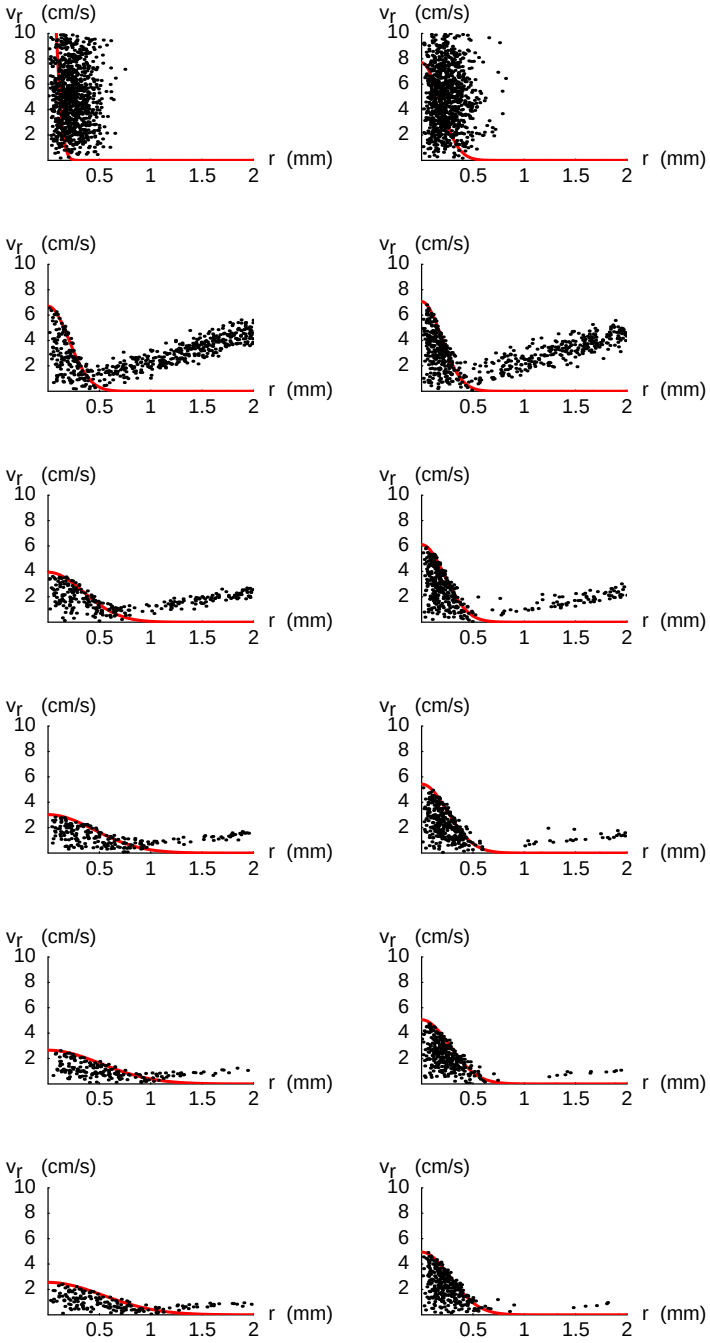

Figure 3.8: Phase-space plots (radial velocity, v_r, versus radial position, r) showing the evolution of atoms within a laser guide for a 100 μm (left column) and 250 μm (right column) beam waist. Proceeding down the page, the times are $t = 0, 42, 85, 127, 169$ and 212 ms. The red line on the plot is the $E = 0$ energy contour.